Binuclear Pt−Tl Bonded Complex with Square Pyramidal Coordination around Pt: A Combined Multinuclear NMR, EXAFS, UV−Vis, and DFT/TDDFT Study in Dimethylsulfoxide Solution

Mihály Purgel,[†,∇] Mikhail Maliarik,[‡] Julius Glaser,[§] Carlos Platas-Iglesias,[∥] Ingmar Persson,[⊥] and Imre Tóth[*,†]

[†]Department of Inorganic and Analytical Chemistry, University of Debrecen, P.O. Box 21, Egyetem tér 1, Debrecen H-4010, Hungary

[‡]Outotec (Sweden) AB, Gymnasievägen 14, P.O. Box 745, SE-031 27 Skellefteå, Sweden

[§]Department of Chemistry, The Royal Institute of Technology (KTH), S-100 44 Stockholm, Sweden

[∥]Departamento de Química Fundamental, Universidade da Coruña, Campus da Zapateira, Alejandro de la Sota 1, 15008 A Coruña, Spain

[⊥]Department of Chemistry, Swedish University of Agricultural Sciences, P.O. Box 7015, SE-750 07 Uppsala, Sweden

[∇]Research group of Homogeneous Catalysis, MTA-DE, University of Debrecen, Egyetem tér 1, Debrecen H-4032, Hungary

Ⓢ *Supporting Information*

ABSTRACT:
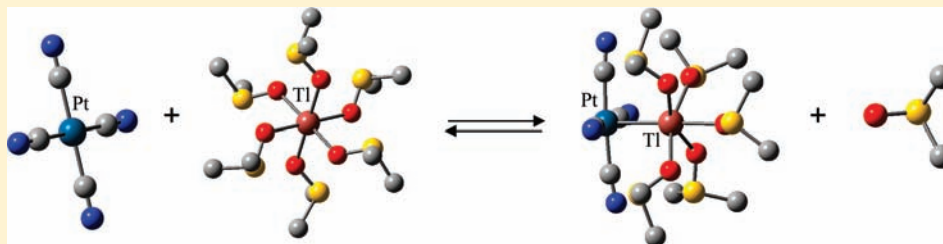
The structure and bonding of a new Pt−Tl bonded complex formed in dimethylsulfoxide (dmso), $(CN)_4Pt-Tl(dmso)_5^+$, have been studied by multinuclear NMR and UV−vis spectroscopies, and EXAFS measurements in combination with density functional theory (DFT) and time dependent density functional theory (TDDFT) calculations. This complex is formed following the equilibrium reaction $Pt(CN)_4^{2-} + Tl(dmso)_6^{3+} \leftrightarrows (CN)_4Pt-Tl(dmso)_5^+ + dmso$. The stability constant of the Pt−Tl bonded species, as determined using ^{13}C NMR spectroscopy, amounts to log $K = 2.9 \pm 0.2$. The $(NC)_4Pt-Tl(dmso)_5^+$ species constitutes the first example of a Pt−Tl bonded cyanide complex in which the sixth coordination position around Pt (in *trans* with respect to the Tl atom) is not occupied. The spectral parameters confirm the formation of the metal−metal bond, but differ substantially from those measured earlier in aqueous solution for complexes $(CN)_5Pt-Tl(CN)_n(H_2O)_x^{n-}$ ($n = 0-3$). The ^{205}Tl NMR chemical shift, $\delta = 75$ ppm, is at extraordinary high field, while spin−spin coupling constant, $^1J_{Pt-Tl} = 93$ kHz, is the largest measured to date for a Pt−Tl bond in the absence of supporting bridging ligands. The absorption spectrum is dominated by two strong absorption bands in the UV region that are assigned to MMCT (Pt → Tl) and LMCT (dmso → Tl) bands, respectively, on the basis of MO and TDDFT calculations. The solution of the complex has a bright yellow color as a result of a shoulder present on the low energy side of the band at 355 nm. The geometry of the $(CN)_4Pt-Tl$ core can be elucidated from NMR data, but the particular stoichiometry and structure involving the dmso ligands are established by using Tl and Pt L_{III}-edge EXAFS measurements. The Pt−Tl bond distance is 2.67(1) Å, the Tl−O bond distance is 2.282(6) Å, and the Pt−C−N entity is linear with Pt−C and Pt···N distances amounting to 1.969(6) and 3.096(6) Å, respectively. Geometry optimizations on the $(CN)_4Pt-Tl(dmso)_5^+$ system by using DFT calculations (B3LYP model) provide bond distances in excellent agreement with the EXAFS data. The four cyanide ligands are located in a square around the Pt atom, while the Tl atom is coordinated in a distorted octahedral fashion with the metal being located 0.40 Å above the equatorial plane described by four oxygen atoms of dmso ligands. The four equatorial Tl−O bonds and the four cyano ligands around the Pt atom are arranged in an alternate geometry. The coordination environment around Pt may be considered as being square pyramidal, where the apical position is occupied by the Tl atom. The optimized geometry of $(CN)_4Pt-Tl(dmso)_5^+$ is asymmetrical (C_1 point group). This low symmetry might be responsible for the unusually large NMR linewidths observed due to *intra*molecular chemical exchange processes. The nature of the Pt−Tl bond has been studied by MO analysis. The metal−metal bond formation in $(CN)_4Pt-Tl(dmso)_5^+$ can be simply interpreted as the result of a $Pt(5d_{z^2})^2 \rightarrow Tl(6s)^0$ donation. This bonding scheme may rationalize the smaller thermodynamic stability of this adduct compared to the related complexes with $(CN)_5Pt-Tl$ entity, where the linear C−Pt−Tl unit constitutes a very stable bonding system.

■ INTRODUCTION

The first Pt—Tl bonded compound, PtTl$_2$(CN)$_4$, was reported by Balch et al.[1] more than 20 years ago. The unusual structure of this compound, which involves two covalent Pt—Tl bonds, and its strong luminescence, prompted several studies of its electronic properties.[2,3] Later, many compounds containing Pt—Tl linkages were reported.[4,5] Pt—Tl bonded compounds can be classified into three different classes depending on the formal oxidation state of the metal ions involved in metal—metal bond formation:[6] (1) 5d^{10}—6s^2 (Pt^0—Tl^I),[7] (2) 5d^8—6s^2 (Pt^{II}—Tl^I),[8,9] and (3) 5d^8—6s^0 or 5d^8—5d^{10} (Pt^{II}—Tl^{III}).[10] One example of a paramagnetic 5d^8—6s^1 (Pt^{II}—Tl^{II}) compound containing the Pt—Tl linkage has also been reported.[11] However, in many cases it is difficult to assign the formal oxidation state of the metal ions involved in metal—metal bond, with it being more correct to give the sum of the formal oxidation states of the two metals instead.[9,12] Concerning compounds of divalent platinum, the Pt—Tl bond becomes shorter when the oxidation state of thallium increases from Tl^I to Tl^{III}, which can be attributed to the decreased size and increased electron-acceptor properties of the thallium ion. Indeed, reaction of Pt^{II} and Tl^{III} cyano complexes in aqueous solution leads to the formation of Pt—Tl bonded complexes of formula (NC)$_5$Pt—Tl(CN)$_n$$^{n-}$ ($n = 0$–3).[13–17] These compounds can be regarded as metastable intermediates in a two-electron transfer reaction between Tl^{III} and Pt^{II}, which leads to Tl^I and Pt^{IV} as final products.[18] The completion of the reaction can be induced both by thermal and optical means, resulting in the cleavage of the metal—metal bond.[19] Similar Pt—Tl bonded compounds of formula (NC)$_5$Pt—Tl(CN)$_n$(dmso)$^{n-}$ ($n = 0$–3) can also be formed in dmso solution.[20] The unusual spectral parameters of these bimetallic compounds have prompted several detailed theoretical studies.[3,4]

In the (NC)$_5$Pt—Tl(CN)$_n$$^{n-}$ series of compounds the fifth axial cyano ligand coordinates to platinum in *trans* position with respect to the metal—metal bond, thereby completing an octahedral six-coordination around platinum. Detailed kinetic studies of the formation reactions of these Pt—Tl bonded cyano complexes showed that they are formed following a similar reaction path that includes the formation of the Pt—Tl bond and the subsequent coordination of the fifth cyano ligand to Pt.[21] A similar coordination environment around Pt is maintained in the (NC)$_5$Pt—Tl(edta)$^{4-}$ complex, where the cyanide ligands coordinated to Tl are replaced by ethylenediaminetetraacetate (edta).[22] An octahedral six-coordination around Pt is also observed in the related Pt—Tl bonded complexes of formula (NC)$_5$Pt—Tl(en)$_{n-1}$ ($n = 1$–3),[20] (NC)$_5$Pt—Tl(phen)$_n$(dmso)$_m$ ($n = 1$, $m = 3$; $n = 2$, $m = 0$),[23] (NC)$_5$Pt—Tl(bipy)$_m$(solv),[24] and (NC)$_5$Pt—Tl(tpp)[25] which have been prepared in dmso solution and contain ethylenediamine (en), 1,10-phenanthroline (phen), 2,2′-bipyridine (bipy), or tetraphenylporphyrin (tpp) ligands coordinated to thallium, respectively. It has been proposed that the bonding in the C$_{ax}$—Pt—Tl pattern of the pseudooctahedral {(NC)$_5$Pt—Tl} unit can be regarded as a three-center four-electron bond as a result of the combination of carbon 2p$_z$, thallium 6s, and platinum 5d$_{z^2}$ orbitals. The presence of the fifth cyanide ligand in the platinum coordination is considered to be a key factor in the stabilization of the {(NC)$_5$Pt—Tl} entity.[3,4]

Indeed, all attempts to form platinum(II)—thallium(III) bonded complexes with the absence of the extra ("fifth") cyanide in aqueous system were unsuccessful. Thus, e.g., the reaction between Pt(CN)$_4$$^{2-}$ and Tl(H$_2$O)$_6$$^{3+}$ complexes in aqueous solution resulted in immediate and quantitative precipitation of low-soluble microcrystalline colored powder with a partially disordered crystal structure.[26] Interestingly, however, when studying a Pt(CN)$_4$$^{2-}$—Tl^{3+}—phen system in dimethylsulfoxide, a stable (NC)$_4$Pt—Tl$_{solv}$$^+$ species could be detected in solution and identified by ^{205}Tl NMR.[23]

In this paper we report a complete study of this new Pt—Tl bonded species, which was prepared by reaction of Pt(CN)$_4$$^{2-}$ with thallium(III) in dmso solution. The formation and stability of (NC)$_4$Pt—Tl(dmso)$_5$$^+$ was investigated by using multinuclear NMR (^{13}C, ^{205}Tl, ^{195}Pt) and UV—vis spectroscopies. The structure of the heterobinuclear species was investigated by using EXAFS measurements in dmso solution. Furthermore, density functional theory (DFT) calculations were used to investigate the structure of the (NC)$_4$Pt—Tl(dmso)$_5$$^+$ species. A molecular orbital analysis was also performed to understand the nature of the Pt—Tl bond. Finally, TDDFT calculations were used to rationalize the absorption spectrum of this compound.

■ EXPERIMENTAL SECTION

Materials. A 1.43 M Tl(ClO$_4$)$_3$ stock solution (containing 2.88 M HClO$_4$) was prepared from TlClO$_4$ by anodic oxidation. The thallium(III) and thallium(I) concentrations were measured by bromatometric titration as described elsewhere.[27] Compound Tl(dmso)$_6$(ClO$_4$)$_3$ was prepared via solvent exchange[28] by addition of 0.7 cm^3 of the 1.43 M Tl(ClO$_4$)$_3$ stock solution into dmso (8 cm^3) in small portions under stirring. The opalescence of the mixture disappeared after addition of a few drops of dmso and light heating. The mixture was further stirred for 25 min resulting in a homogeneous solution with $c \sim 84$ mmol/dm^3 thallium(III). Small white crystals were formed after one day at ambient temperature. The crystals were separated on a glass filter, washed with dmso, and dried under an air-flow. The crystals were kept in vacuum desiccators. The yield was 47%. The purity of the solid was checked by measuring the thallium content by ICP-AAS. The ^{205}Tl NMR spectrum in dmso showed only one signal at 1902 ppm due to Tl(dmso)$_6$$^{3+}$,[28] while no thallium(I) impurities could be detected. Only fresh dmso solutions were used throughout this study, as after some time decomposition of the dmso can occur. Thus, dmso (Aldrich) was either used within one week after purchase or purified by vacuum-distillation prior to use. *Warning! Although we have experienced no difficulties with the perchlorate salts, these should be regarded as potentially explosive and handled with care.[29] Therefore, the maximal amount of Tl(dmso)$_6$(ClO$_4$)$_3$ handled was only 200–300 mg because of the risk of working with heavy metal perchlorates in organic solvents. Solutions containing cyanides should also be handled with care due to possible emission of poisonous gases: HCN in acidic medium, or (CN)$_2$ in oxidizing medium.*

K$_2$Pt(CN)$_4$·3H$_2$O was purchased from Aldrich, while Na$_2$Pt(CN)$_4$·3H$_2$O was prepared by reacting K$_2$PtCl$_4$ and 6 equiv of NaCN. Solid NaCN was added to a saturated (0.18 M) aqueous solution of K$_2$PtCl$_4$, with the yellow solution becoming colorless after mixing. The solution was evaporated to half of its original volume on a steam bath, allowed to cool down to room temperature, and left to stand overnight, which resulted in the formation of the desired compound as a white powder. The preparation of labeled Na$_2$Pt(^{13}CN)$_4$·3H$_2$O followed the same procedure by using Na^{13}CN (Cambridge Isotopes).

Methods. *NMR Measurements.* ^{13}C NMR spectra were recorded on Bruker Avance 500 and DRX500 spectrometers equipped with 5 mm BBO probes at 25 ± 0.5 °C. Typical acquisition parameters were SF = 125 MHz, pulse length 10 μs (30°), repetition time 3 s. The chemical shift was calibrated to TMS ($\delta = 0$ ppm) as external standard.

^{205}Tl NMR spectra were recorded on a Bruker DMX500 spectrometer at 25 ± 0.5 °C. Typical acquisition parameters were SF = 288.6

Table 1. Mean Bond Distances, d/Å, Debye–Waller Parameters, σ^2/Å^2, the Number of Distances, N, Obtained from EXAFS Measurements for the Dimethylsulfoxide Solvated Tetracyanoplatinate(II)–Thallium(III) Complex in Solution at Ambient Room Temperature

interaction	N	d	σ^2
Solution 1 Platinum L$_{III}$-Edge			
Pt–Tl	1	2.659(1)	0.0056(1)
Pt–C	4	1.969(2)	0.0043(1)
Pt···N	4	3.094(2)	0.0089(3)
Pt–Tl–C	16	3.39(1)	0.013(1)
MS	3 × 4	3.92(1)	
Solution 1 Thallium L$_{III}$-Edge			
Tl–Pt	1	2.667(2)	0.0053(3)
Tl–O	5.5	2.259(4)	0.0195(5)
Tl···S	5.5	3.288(9)	0.038(2)
Tl–O–S	11	3.472(3)	0.0043(3)
MS	3 × 5.5	4.49(4)	0.039(56)
Solution 2 Platinum L$_{III}$-Edge			
Pt–Tl	1	2.659(1)	0.0056(1)
Pt–C	4	1.969(1)	0.0055(2)
Pt···N	4	3.098(2)	0.0104(2)
Pt–Tl–C	16	3.39(1)	0.015(1)
MS	3 × 4	3.92(1)	
Solution 2 Thallium L$_{III}$-Edge			
Tl–Pt	1	2.677(4)	0.0096(5)
Tl–O	5	2.282(2)	0.0050(2)
Tl···S	5	3.327(5)	0.0140(7)
Tl–O–S	10	3.526(3)	0.0027(3)
MS	3 × 5	4.54(4)	0.019(5)

MHz, pulse length 10 μs (30°), repetition time 2 s. We used a 50 mM TlClO$_4$ aqueous solution as external standard ($\delta = -4.7$ ppm, extrapolated from $\delta = 0$ ppm for "infinite dilution"). Some [205]Tl NMR spectra were also recorded on a Bruker Avance 360 spectrometer (SF = 207.8 MHz), where the XBB channel of a 500 MHz 10 mm BBO probe was tuned to the frequency of the [205]Tl nucleus.

[195]Pt NMR spectra were recorded on Bruker Avance 500 spectrometer at 25 ± 0.5 °C. Typical acquisition parameters were SF = 96.7 MHz, pulse length 10 μs (30°), repetition time 2 s. The chemical shift calibration was performed by using Na$_2$PtCl$_6$ or Na$_2$Pt(CN)$_4$ solutions as external standards, $\delta = 4533$ ppm and $\delta = -213$ ppm, respectively, referring to Ξ ([195]Pt) = 21.4 MHz.

UV–Vis Measurements. The measurements were done with a Varian Cary 1E spectrophotometer at room temperature using 1 mm and 0.01 mm quartz cells.

EXAFS Measurements. Platinum and thallium L$_{III}$-edge X-ray absorption spectra were recorded at the wiggler beamline I811 at MAX-lab, Lund University, Sweden. The EXAFS station was equipped with a Si[111] double crystal monochromator. MAX-lab operated at 1.5 GeV and a maximum current of 250 mA. The data collections were performed in transmission mode and at ambient temperature. Higher order harmonics were reduced by detuning the second monochromator to 50% of maximum intensity at the end of the scans. The solutions were contained in cells with 1.5 mm Teflon spacers and 6 μm polypropylene film windows. The energy scales of the X-ray absorption spectra were calibrated by assigning the first inflection point of the L$_{III}$-edge of a platinum foil and powdered selenium (the K-edge absorption edge of

selenium and the L$_{III}$-edge absorption of platinum are identical) to 11 563 and 12 658 eV, respectively.[30] For each sample two 90 min scans were averaged on both edges, giving satisfactory data (k^3-weighted) in the k range 3–13.5 and 2–11 Å^{-1} for platinum and thallium, respectively. The EXAFSPAK program package was used for the data treatment.[31]

The standard deviations given for the refined parameters in Table 1 are obtained from k^3 weighted least-squares refinements of the EXAFS function $\chi(k)$, and do not include systematic errors of the measurements. These statistical error estimates provide a measure of the precision of the results and allow reasonable comparisons, e.g., of the significance of relative shifts in the distances. However, the variations in the refined parameters, including the shift in the E_o value (for which $k = 0$), using different models and data ranges, indicate that the absolute accuracy of the distances given for the separate complexes is within ±0.01 to 0.02 Å for well-defined interactions. The "standard deviations" given in the text have been increased accordingly to include estimated additional effects of systematic errors.

Two different solutions were used in EXAFS experiments, one containing excess of thallium(III) (Tl(dmso)$_6$$^{3+}$) (solution 1) and another containing excess of platinum(II) (Pt(CN)$_4$$^{2-}$) (solution 2). The samples were prepared in Lund directly before the measurements to avoid any decomposition of the complex. For solution 1, 116 mg (0.12 mmol) of Tl(dmso)$_6$(ClO$_4$)$_3$ and 26 mg (0.060 mmol) of K$_2$Pt(CN)$_4$·3H$_2$O were dissolved in 1.5 mL of dmso under rigorous stirring for 4–5 min to get a homogeneous solution. Solution 2 was prepared following an identical procedure from 52 mg of K$_2$Pt(CN)$_4$·3H$_2$O (0.12 mmol) and 58 mg of Tl(dmso)$_6$(ClO$_4$)$_3$ (0.06 mmol) in 1.5 mL of dmso. The total concentrations of the solutions were 80 mM thallium(III) and 40 mM Pt(CN)$_4$$^{2-}$ (solution 1) and 40 mM thallium(III) and 80 mM Pt(CN)$_4$$^{2-}$ (solution 2). Under these conditions the Pt–Tl bound species is expected to represent 97% of the maximum amount attainable (40 mM, see speciation diagrams in Figure S1, Supporting Information).

The samples were sent back to Debrecen after EXAFS measurements, and their compositions were investigated by [205]Tl NMR (20 days after their preparation) to check whether the samples suffered some change by radiolysis. The [205]Tl NMR spectra of these solutions showed that the thallium content in solution 1 was distributed between three sites: about 60% of the dmso solvated (CN)$_4$Pt–Tl$^+$ complex, 30% Tl(dmso)$_6$$^{3+}$, and 10% dimethylsulfoxide solvated thallium(I). The corresponding figures for solution 2 were about 55% dmso solvated thallium(I), 40% of the dmso solvated (CN)$_4$Pt–Tl$^+$ complex, and 5% of an unknown thallium(III) species. These data confirmed remarkable decomposition of the samples caused by the X-ray beam, but the dmso solvated (CN)$_4$Pt–Tl$^+$ complex remained the dominating scattering entity in both samples used for thallium and platinum L$_{III}$-edge X-ray absorption.

Computational Methods. All calculations were performed employing hybrid DFT with the B3LYP exchange-correlation functional,[32,33] and the Gaussian 03 package (Revision C.01).[34] Full geometry optimizations of the Pt(CN)$_4$$^{2-}$, (CN)$_4$Pt–Tl(dmso)$_5$$^+$, (CN)$_4$(dmso)Pt–Tl(dmso)$_5$$^+$, and (CN)$_4$(dmso)Pt–Tl(dmso)$_4$$^+$ systems were performed in vacuo by using the 6-31G(d) basis set for C, H, N, O, and S atoms. For Pt and Tl we used the Ermler–Christiansen relativistic effective core potential (RECP) basis set.[35] For Pt, 60 electrons are included in the core, with the remaining valence space of Pt (5s, 5p, 5d, 6s) represented by an uncontracted (5s5p4d) basis. For Tl, 68 core electrons were replaced by the RECP, with the remaining valence space of Tl (5d, 6s, 6p) represented by an uncontracted (3s3p4d) basis. It has been demonstrated that this ECP provides reliable results for Pt[36] and Tl complexes.[37] Compared to all-electron basis sets, ECPs account to some extent for relativistic effects, which are believed to become important for the elements from the fourth row of the periodic table. Spin–orbit coupling effects were not taken into account in the present work. No symmetry constraints have been imposed during the optimizations. The default values for the integration grid ("fine") and the SCF energy
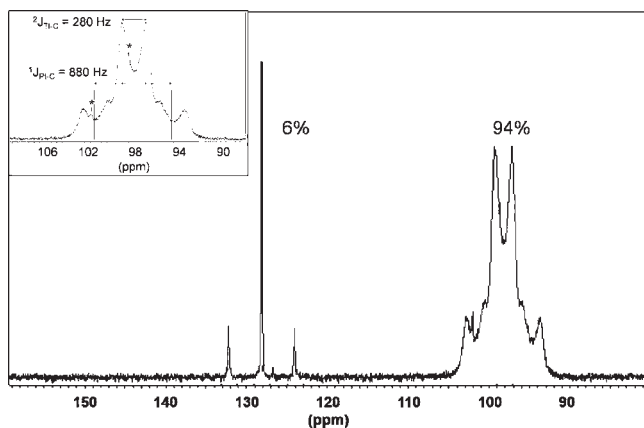
Figure 1. 125 MHz ^{13}C NMR spectrum of a dmso solution containing Pt(^{13}CN)$_4$$^{2-}$ (40 mM) and Tl(dmso)$_6$$^{3+}$ (80 mM). The insert shows the deconvolution of the broad signal at 98 ppm with the $^1J_{Tl-C}$ and $^1J_{Pt-C}$ spin−spin coupling constants of the complex. (Asterisks indicate nonidentified minor species.)

convergence criteria (10^{-6}) were used. The stationary points found on the potential energy surfaces as a result of the geometry optimizations have been tested to represent energy minima rather than saddle points via frequency analysis. Test calculations performed on the (CN)$_5$Pt–Tl(dmso)$_4$ system, whose X-ray structure has been reported,[20] show that our computational approach reproduces fairly well the solid state structure of this class of compounds (Table S1, Supporting Information). Our calculations overestimate the Pt−Tl distance by only ca. 0.04 Å, and the Tl−O distances by ca. 0.06−0.09 Å. The calculated Pt−C distances are in excellent agreement with the experimental values (within 0.02 Å).

In dmso solution solvation energies and free energies of reaction were calculated from solvated single-point energy calculations on the geometries optimized in vacuo. Solvent effects were evaluated by using the polarizable continuum model (PCM), in particular employing the integral equation formalism variant (IEF-PCM).[38] In line with the united atom topological model (UATM),[39] the solute cavity is built as an envelope of spheres centered on atoms or atomic groups with appropriate radii. Each sphere is subdivided in 60 initial tesserae in pentakisdodecahedral patterns. Calculations were performed using an average area of 0.2 Å^2 for all the finite elements (tesserae) used to build the solute cavities. Final free energies of reaction include both electrostatic and nonelectrostatic contributions. Time-dependent density functional theory (TDDFT)[40] was used for the calculation of the 20 lowest energy electronic transitions of the (CN)$_4$Pt−Tl(dmso)$_5$$^+$ system in dmso solution. The absorption spectra were simulated according to the following equations:[41]

$$\varepsilon(E) = \sum_{(i)} a_i \exp\left(-2.773(E - E_i)^2/\Delta_{1/2}{}^2\right) \quad (1)$$

$$a_i = 2.174 \times 10^9 f_i/\Delta_{1/2} \quad (2)$$

Here the sum runs over all TDDFT-calculated transitions with energies E_i and oscillator strengths f_i. The half-bandwidths, $\Delta_{1/2}$, were assumed to be equal to 3600 cm^{-1} on the basis of the experimental half-bandwidth of the band observed at 356 nm, which was purely belonging to the metal−metal bound species.

■ RESULTS AND DISCUSSION

Reaction of Pt(CN)$_4$$^{2-}$ with Tl(dmso)$_6$$^{3+}$ in Dimethylsulfoxide Solution. Addition of the Tl(dmso)$_6$$^{3+}$ to a solution of Pt(^{13}CN)$_4$$^{2-}$
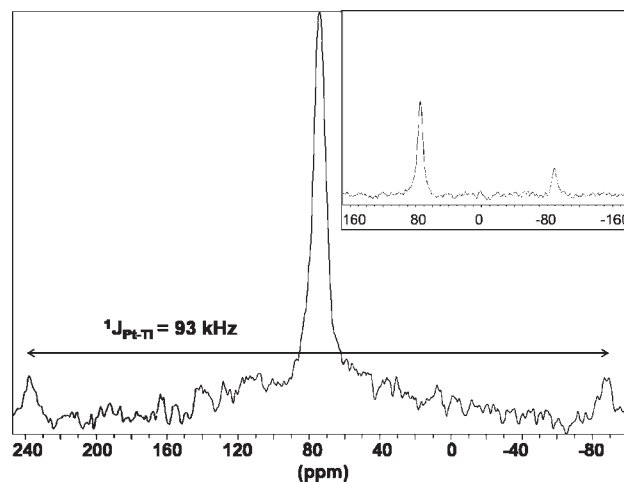
Figure 2. Fraction of a ^{205}Tl NMR spectrum in dmso solution containing Pt(^{13}CN)$_4$$^{2-}$ (40 mM) and Tl(dmso)$_6$$^{3+}$ (80 mM). The insert shows the fragment of the spectra recorded with carrier frequency at 0 ppm (see ref 42).

in dmso solution causes important changes in the ^{13}C NMR spectrum of the solution. Upon Tl(dmso)$_6$$^{3+}$ addition, the intensity of the signal due to Pt(CN)$_4$$^{2-}$ at 129 ppm gradually decreases, while the formation of a new relatively broad signal at 98 ppm is observed (Figure 1). This signal can be described as a doublet due to coupling to ^{205}Tl ($^2J_{Tl-C}$ = 280 Hz) flanked by satellites due to coupling to ^{195}Pt (natural abundance 33.8%, $I = {}^1/_2$, $^1J_{Pt-C}$ = 880 Hz). Both the chemical shift value and the Pt−C coupling constant are typical of Pt−cyano complexes.[18] The coupling scheme observed for the signal at 98 ppm is consistent with the bonding of Pt to one Tl atom in the species.

The ^{205}Tl NMR spectrum of a dmso solution containing Pt(^{13}CN)$_4$$^{2-}$ (40 mM) and Tl(dmso)$_6$$^{3+}$ (80 mM) shows a singlet at 75 ppm flanked by satellites due to coupling to ^{195}Pt (Figure 2). This result unambiguously demonstrates the formation of the Pt−Tl bond. The two satellites together with the central uncoupled peak should give an intensity pattern 1:3.9:1 for a complex with a 1:1 Pt/Tl stoichiometry.[42]

^{205}Tl NMR chemical shifts cover a region of more than 5000 ppm and are very sensitive to the oxidation state of thallium. For instance, in aqueous solutions the chemical shifts of Tl(III)-containing compounds fall within the range +1800 to +3600 ppm, while for Tl(I) compounds chemical shifts are normally found in the interval −200 to +200 ppm.[43] The chemical shift observed in the present case (75 ppm) is very different from that found for Tl(dmso)$_6$$^{3+}$ (1891 ppm)[28] and even lower than that reported for TlClO$_4$ in dmso (361 ppm).[24] The value observed is also very different compared to that measured (887 ppm)[26] for (CN)$_5$Pt−Tl(dmso)$_4$.[20] This result may suggest an unusually low formal oxidation state for the thallium ion in this bimetallic species.

The observed $^1J_{Pt-Tl}$ coupling constant (93 kHz) is one of the largest reported so far in the literature, and the largest measured to date for a Pt−Tl compound without supporting bridging ligands. The important differences observed for $^1J_{Pt-Tl}$ coupling constants of different Pt−Tl compounds can be attributed to varying proportions of thallium 6s character in the metal−metal bond.[14] Indeed, a substantial participation of Tl s electrons in bond formation is expected to be reflected in large $^1J_{Pt-Tl}$ coupling constants. Thus, the large coupling constant observed
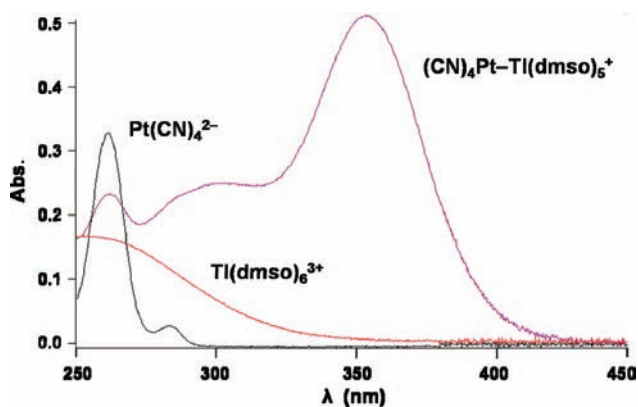
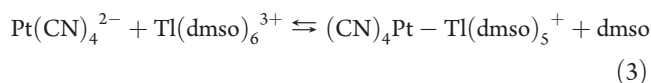**Figure 3.** Typical absorption spectra of the dmso solutions of the reactants and the metal−metal bonded complex: $c_{Pt(CN)_4^{2-}} = 20$ mM (black), $c_{Tl(dmso)_6^{3+}} = 20$ mM (red), and $c_{Pt(CN)_4^{2-}} = c_{Tl(dmso)_6^{3+}} = 20$ mM (violet); $l = 0.01$ mm.

in the present case suggests a very important participation of the valence Tl 6s orbital in the formation of this particular Pt−Tl bond.

Unfortunately, attempts to find the signal due to the bimetallic species in the ^{195}Pt NMR spectrum have been unsuccessful, probably because the signal is too broad to be detected due to exchange phenomena in dmso solution. The relatively broad signals observed in the ^{13}C and ^{205}Tl NMR spectra support this hypothesis. However, the signal due to the $Pt(CN)_4^{2-}$ species in the ^{13}C NMR spectra is quite narrow (Figure 1), indicating that an *inter*molecular exchange process between $(CN)_4Pt-Tl(dmso)_5^+$ and $Pt(CN)_4^{2-}$ is not responsible for observed line broadening. Thus, an *intra*molecular exchange process is probably responsible for the broad signals observed in the ^{13}C NMR spectra and the absence of detectable resonances in the ^{195}Pt NMR spectrum.[44]

The ^{13}C and ^{205}Tl NMR spectra, together with the EXAFS and DFT results presented below, are consistent with the following reaction in dmso solution:

$$Pt(CN)_4^{2-} + Tl(dmso)_6^{3+} \rightleftharpoons (CN)_4Pt - Tl(dmso)_5^+ + dmso \tag{3}$$

Since the concentration of solvent dmso is effectively constant, the equilibrium constant corresponding to eq 3 can be written as

$$K = \frac{[(CN)_4Pt - Tl(dmso)_5^+]}{[Pt(CN)_4^{2-}][Tl(dmso)_6^{3+}]} \tag{4}$$

Square brackets mean equilibrium concentrations in eqs 4−6. In practice only the central peaks of the narrow signal for $Pt(^{13}CN)_4^{2-}$ at 129 ppm could be integrated quantitatively, and therefore, the equilibrium concentrations of the other species were calculated using the following mass balance equations:

$$c_{Pt} = [(CN)_4Pt - Tl(dmso)_5^+] + [Pt(CN)_4^{2-}] \tag{5}$$

$$c_{Tl} = [(CN)_4Pt - Tl(dmso)_5^+] + [Tl(dmso)_6^{3+}] \tag{6}$$

A log K value of 2.9 ± 0.2 has been obtained from the analysis of the ^{13}C NMR titration data (see Figure S2, Supporting Information).

The reaction between $Pt(CN)_4^{2-}$ and $Tl(dmso)_6^{3+}$ has also been followed by using UV−vis spectroscopy (Figure 3). Addition of 1 equiv of $Tl(dmso)_6^{3+}$ to a 20 mM solution of $Pt(CN)_4^{2-}$ in dmso results in the formation of new bands with maxima at 310 and 355 nm. The relatively high intensity of these bands ($\varepsilon \sim 4 \times 10^4$ M^{-1} cm^{-1} at 355 nm) is typical of charge transfer (CT) transitions. The low energy tail of this band extents to the visible region of the spectrum, and it is responsible for the yellow color of the solutions containing the $(CN)_4Pt-Tl(dmso)_5^+$ complex. The maximum of this CT band is observed at lower energy than in the case of the $(NC)_5Pt-Tl(dmso)_x^+$ species, for which the absorption maximum has been located at 297 nm ($\varepsilon = 2 \times 10^4$ M^{-1} cm^{-1}).[26] A stability constant of log $K = 3.38 \pm 0.02$, defined by eq 4, has also been determined by spectrophotometry via systematic variation of the ratio of reactants, $Pt(CN)_4^{2-}$ and $Tl(dmso)_6^{3+}$ (see Figure S3, Supporting Information).

■ EXAFS MEASUREMENTS

Composition of the Studied Solutions. The structure of the dmso solvated $(CN)_4Pt-Tl^+$ complex was investigated by using EXAFS measurements. The two solutions studied, denoted as solutions 1 and 2, contained $c_{Pt} = 40.0$ and 80.0 mmol dm^{-3}, and $c_{Tl} = 80.0$ and 40.0 mmol dm^{-3}, respectively, as described in the Experimental Section. The structures of dmso solvated thallium(III) and thallium(I) ions have been reported previously.[45] The dmso solvated thallium(III) ion is six-coodinate with a regular octahedral environment and dmso binding through oxygen with mean Tl−O and Tl···S distances of 2.22(1) and 3.33(2) Å, giving a Tl−O−S bond angle of 124(2)° in dmso solution.[28] The structure of solid $Tl(OS(CH_3)_2)_6-(ClO_4)_3$ displays the same Tl−O bond distances at both room temperature and 10 K, but the Tl−O−S bond angles are somewhat smaller (120°). The dmso solvated thallium(I) ion has a diffuse solvation shell with two groups of weakly bound solvent molecules at 2.66(4) and 3.18(6) Å in dmso solution.[28] The scattering effect in an EXAFS study of dmso solvated thallium(I), based on the Debye−Waller factors obtained in the LAXS experiments, is ca. 10% of the scattering effect of the dmso solvated thallium(III) ion at low k values, and negligible at high k values. This means that the contribution to the EXAFS data from the thallium(I) ion that might be formed during the data collection in solution 1 (see Experimental Section) is negligible in comparison to the contribution from the dmso solvated thallium(III) and $(CN)_4Pt-Tl^+$ complexes. The contribution from the solvated thallium(I) ion in solution 2 is also not sufficiently important to be independently observed. Therefore, the contributions to the thallium L_{III}-edge EXAFS data in this study are solely from the dmso solvated thallium-(III) and $(CN)_4Pt-Tl^+$ complexes.

Structure of the Dimethylsulfoxide Solvated $(CN)_4Pt-Tl^+$ Complex. The thallium L_{III}-edge EXAFS data show a Pt−Tl bond distance of 2.67(1) Å in solution 1. The refined mean Tl−O bond distance is 0.04 Å longer than in the dmso solvated thallium(III) ion, and has a large Debye−Waller factor, 0.020 Å^2. The difference in the Tl−O bond distances in the $Tl(dmso)_6^{3+}$ and $(NC)_4Pt-Tl(dmso)_5^+$ complexes is, however, too small to be separated in the refinements of the EXAFS data. Assuming that the observed mean Tl−O bond distance, 2.259 Å, is a weighted mean value in the $Tl(dmso)_6^{3+}$ (2.220 Å) and $(NC)_4Pt-Tl(dmso)_5^+$ complexes, this gives a Tl−O bond distance in the latter of 2.284 Å, partly explaining the large Debye−Waller factor
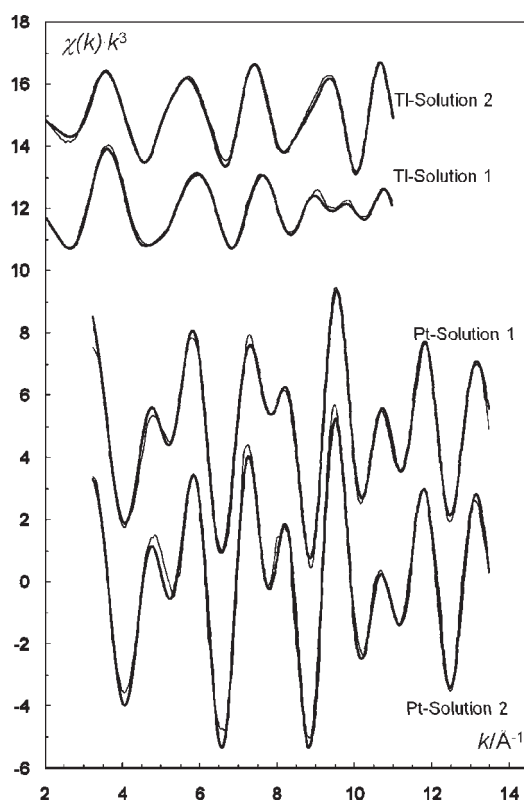
Figure 4. Fit of k^3-weighted EXAFS data of dmso solutions of tetracyanoplatinate(II)—thallium(III), platinum L_{III}-edge data solution 1 (no offset), solution 2 (offset 5.0); and thallium L_{III}-edge data solution 1, (offset 12.0), solution 2 (offset 15.0).
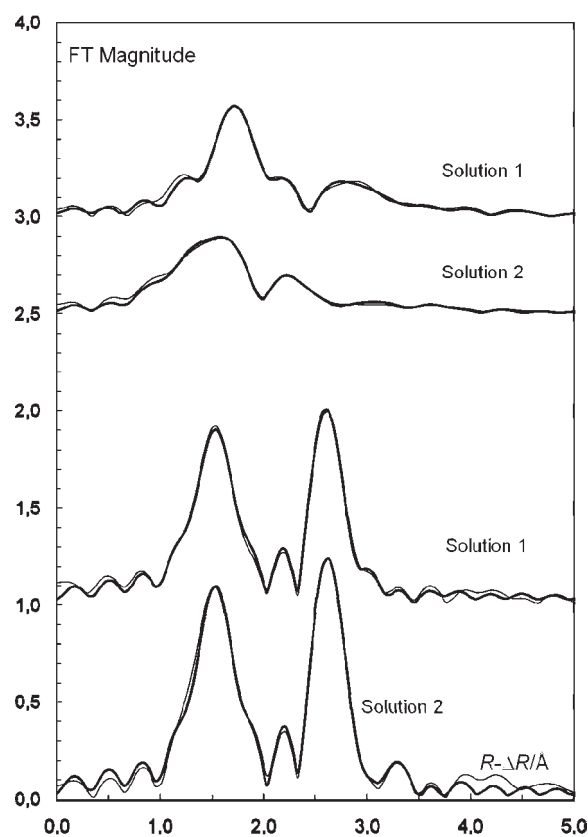

Figure 5. Fourier transforms of k^3-weighted EXAFS data of dmso solutions of tetracyanoplatinate(II)—thallium(III), platinum L_{III}-edge data solution 1 (no offset), solution 2 (offset 1.0); and thallium L_{III}-edge data solution 1, (offset 2.5), solution 2 (offset 3.0).

(Table 1). The observed $Tl\cdots S$ single scattering and $Tl-O-S$ three-leg scattering are consistent with a $Tl-O-S$ scattering angle of 120°. The linear TlO_6 and $-TlO_5$ inner-core multiple scattering distances at double $Tl-O$ bond distance are observed at the expected distances supporting a regular octahedral configuration around thallium in both $Tl(dmso)_6{}^{3+}$ and $(NC)_4Pt-Tl(dmso)_5{}^+$. The thallium L_{III}-edge EXAFS data of solution 2 refer solely to the $(NC)_4Pt-Tl(dmso)_5{}^+$ complex. The Pt—Tl bond distance is 2.677(4) Å, and the Tl—O bond distance is 2.282(2) Å, which is in excellent agreement with the extrapolated bond length from solution 1. The $Tl\cdots S$ single scattering and $Tl-O-S$ three-leg scattering distances give a $Tl-O-S$ scattering angle of 120°. The fit of the thallium L_{III}-edge EXAFS data and Fourier transforms of solutions 1 and 2 are given in Figures 4 and 5, respectively.

The platinum L_{III}-edge EXAFS data of solutions 1 and 2 are almost identical in spite of the excess of $Pt(CN)_4{}^{2-}$ present in solution 2. The Pt—Tl bond distance is 2.659(5) Å in both solutions, which is within the limits of error the same as that observed in the Tl EXAFS data (see above). The Pt—C bond and $Pt\cdots N$ distances, 1.969(6) and 3.096(6) Å, point to a linear Pt—C—N bond, and a bond distance in agreement with earlier observations. The fit of the Pt L_{III}-edge EXAFS data and Fourier transforms of solutions 1 and 2 are given in Figures 4 and 5, respectively.

The observed structure of the $(NC)_4Pt-Tl(dmso)_5{}^+$ complex is consistent with a similar structure of hydrated $(NC)_5Pt-Tl(OH_2)_m{}^+$ complexes in aqueous solution.[46] The Pt—Tl bond distance is slightly longer in the dmso solvated complex due to

stronger solvation of the soft thallium, and/or to different character of Pt—Tl bonding, see below; the D_S values for water and dmso are 18 and 27, respectively.[47] The Pt—C bond distances are slightly shorter in this complex as only four cyanide ions bind to platinum in comparison to five-coordination in the previously studied complexes in water. The Tl—O bond distances are significantly longer in the $(NC)_4Pt-Tl(dmso)_5{}^+$ complex than in $Tl(dmso)_6{}^{3+}$ ion, 0.06 Å, which may indicate an oxidation number of thallium in the metal—metal complex that is (somewhat) lower than three. The Pt—C bond distance is slightly shorter, ca. 0.02 Å, than in $Pt(CN)_4{}^{2-}$ complexes in the solid state,[48] indicating an oxidation number higher than two.

DFT Optimized Geometries. Aiming to obtain information on the structure of the Pt—Tl complex formed upon reaction of $Pt(CN)_4{}^{2-}$ and $Tl(dmso)_6{}^{3+}$ in dmso solution, we have performed geometry optimizations on the $(CN)_4Pt-Tl(dmso)_5{}^+$ (A) system by using the DFT calculations (B3LYP model). Furthermore, we have also explored a possible coordination of a dmso ligand to the Pt center by performing calculations on the $(CN)_4(dmso)Pt-Tl(dmso)_5{}^+$ (B) and $(CN)_4(dmso)Pt-Tl(dmso)_4{}^+$ (C) systems. The optimized geometries for these species are shown in Figure 6. The three bimetallic species present short Pt—Tl distances amounting to 2.735 (A), 2.672 (B), and 2.619 (C) Å. In addition to the Pt—Tl linkage, the Pt atom is bonded to four carbons of the cyanide ligands in the three species. In species B and C, a dmso ligand is coordinated to Pt, while this is not the case for species A.
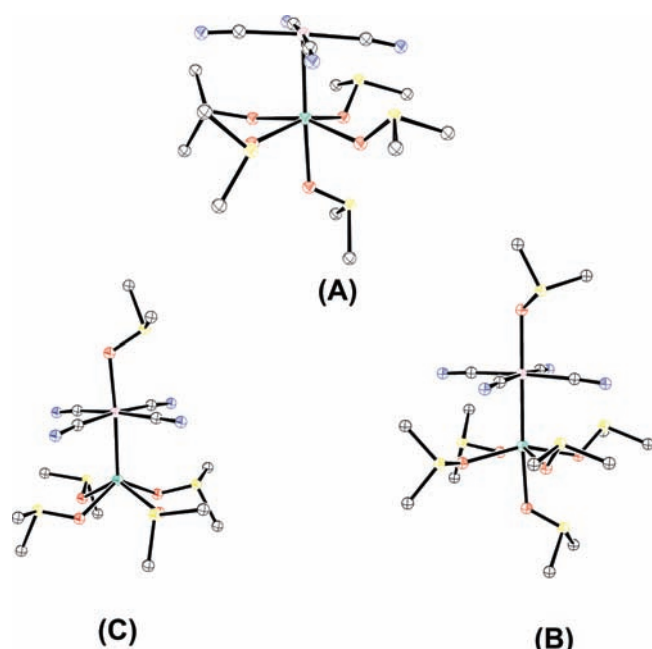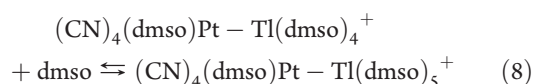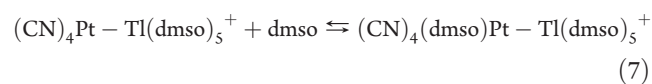
Figure 6. Optimized geometries of the $(CN)_4Pt-Tl(dmso)_5^+$ (A), $(CN)_4(dmso)Pt-Tl(dmso)_5^+$ (B), and $(CN)_4(dmso)Pt-Tl(dmso)_4^+$ (C) systems.

The relative free energies of the A, B, and C species were determined in vacuo by calculating the free energy variation for reactions 7 and 8:

$$(CN)_4Pt-Tl(dmso)_5^+ + dmso \rightleftharpoons (CN)_4(dmso)Pt-Tl(dmso)_5^+ \tag{7}$$

$$(CN)_4(dmso)Pt-Tl(dmso)_4^+ + dmso \rightleftharpoons (CN)_4(dmso)Pt-Tl(dmso)_5^+ \tag{8}$$

The free energies calculated for eqs 7 and 8 amount to -12.5 and -11.2 kJ mol^{-1}, respectively. These results highlight the tendency of a dmso ligand to coordinate to the Pt center in the gas phase. In order to evaluate the solvent effects on the relative stability of these species, we have determined the free energy variations for these reactions in dmso solution. In these calculations the effect of the bulk solvent was included by using the polarizable continuum model (PCM). Our results show that the inclusion of solvent effects dramatically affects the free energies for eqs 7 and 8, which amount to 62.94 and 30.51 kJ mol^{-1}, respectively. Thus, our calculations predict that the $(CN)_4Pt-Tl(dmso)_5^+$ species is the most stable one in dmso solution among the three geometries investigated, in nice agreement with the EXAFS data described above. This is a consequence of the very different dmso solvation free energies calculated for the three species, which amount to -70.38 (A), -3.69 (B), and -36.63 (C) kJ mol^{-1}.

The calculated Pt$-$Tl distance in $(CN)_4Pt-Tl(dmso)_5^+$ (2.735 Å) is $\sim$0.06 Å longer than the experimental one obtained from EXAFS measurements. The averaged Pt$-$C bond distance amounts to 2.014 Å, only 0.04 Å longer than that obtained from our EXAFS measurements in dmso solution. The calculated Tl$-$O distances (average at 2.306 Å) are also in excellent agreement with the experimental values. The four cyanides are
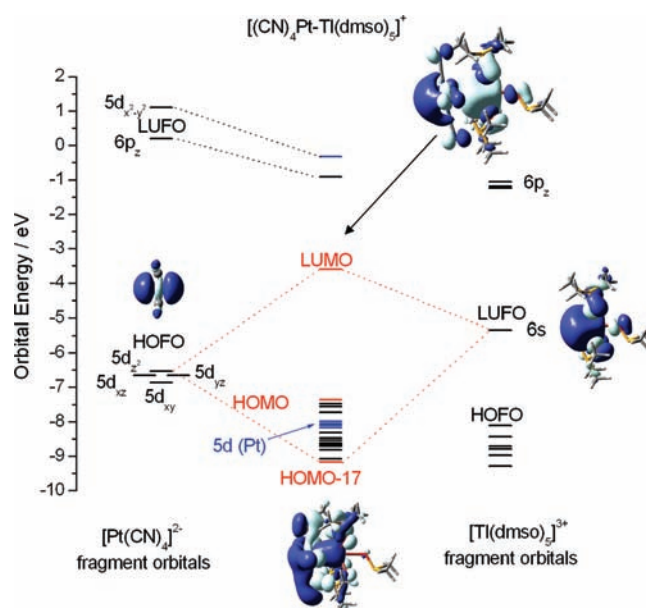

Figure 7. Orbital interaction diagram obtained for $(NC)_4Pt-Tl(dmso)_5^+$ using DFT calculations; $Pt(CN)_4^{2-}$ and $Tl(dmso)_5^{3+}$ are interacting fragments (both in closed-shell singlet spin configuration).

Table 2. Partial Molecular Orbital Compositions (%) in the Ground State for $(NC)_4Pt-Tl(dmso)_5^+$ Obtained in Dimethylsulfoxide Solution (PCM Model) from Mulliken Population Analysis

orbital	energy (eV)	dmso	Tl	CN$^-$	Pt
LUMO+2	−0.320	26.7	−0.2	30.4	43.1
LUMO+1	−0.929	34.8	19.3	31.4	14.5
LUMO	−3.602	28.1	42.9	12.2	16.7
HOMO	−7.363	84.4	0.9	11.1	3.5
HOMO−1	−7.479	91.5	1.5	1.3	5.8
HOMO−2	−7.559	79.6	1.8	13.7	4.9
HOMO−3	−7.722	78.6	1.7	13.4	6.4
HOMO−4	−7.987	58.7	2.2	16.8	22.4
HOMO−5	−8.056	24.1	0.7	45.5	29.7
HOMO−6	−8.113	21.5	0.8	48.8	28.8
HOMO−7	−8.178	25.3	0.6	47.7	26.4
HOMO−8	−8.323	90.6	0.5	4.3	4.5
HOMO−9	−8.471	78.6	1.8	13.7	5.8
HOMO−10	−8.537	77.8	0.6	20.4	1.3
HOMO−11	−8.621	34.0	1.4	60.5	4.2
HOMO−12	−8.658	77.7	2.3	19.1	1.3
HOMO−13	−8.667	48.7	1.5	46.4	3.3
HOMO−14	−8.717	58.4	1.8	38.4	1.4
HOMO−15	−8.812	5.6	0.3	92.9	1.2
HOMO−16	−9.071	12.1	1.2	85.5	1.2
HOMO−17	−9.166	22.4	6.9	49.5	21.1

located in a square plane around the Pt atom. The coordination of the Tl atom can be described as a distorted octahedron with the metal ion being located 0.40 Å above the equatorial plane built by four oxygen atoms of dmso ligands. The four equatorial Tl$-$O bonds and the four cyano ligands coordinated to the platinum atom in the Pt$-$Tl complex are arranged in an alternate

geometry. The coordination environment around Pt may be considered as being square pyramidal, where the apical position is occupied by the Tl atom.

Metal−Metal Bonding in $(NC)_4Pt−Tl(dmso)_5^+$ and $(NC)_5Pt−Tl(dmso)_4$. Aiming to obtain information about the nature of the Pt−Tl bond in $(CN)_4Pt−Tl(dmso)_5^+$ we have performed an MO analysis in dmso solution (PCM model). For this purpose, we have chosen a local coordinate system in which the z axis is aligned along with the Pt−Tl bond, with the x and y axis each containing the Pt atom and two C atoms of cyanide ligands in *trans* positions. Figure 7 shows an orbital interaction diagram for $(CN)_4Pt−Tl(dmso)_5^+$ in which $Pt(CN)_4^{2-}$ and $Tl(dmso)_5^{3+}$ are the interacting fragments, while Table 2 shows the MO compositions relevant to the interpretation of the Pt−Tl bond and the electronic absorption spectrum. For the $Pt(CN)_4^{2-}$ fragment we obtain the following ordering of the energies of the 5d orbitals: $d_{x^2-y^2} \gg d_{z^2} > d_{xz}, d_{yz} > d_{xy}$. This is the expected ordering predicted by the simple crystal field or angular overlap model, except for the reversal order of the d_{xz}, d_{yz}, and d_{xy} orbitals due to their mixing with the CN^- π orbitals.[49] The highest occupied fragment orbital (HOFO) of the $Pt(CN)_4^{2-}$ fragment (74.0% Pt $5d_{z^2}$) and the LUFO of $Tl(dmso)_5^{3+}$ (47.2% Tl 6s) are involved in Pt−Tl bond formation, giving rise to HOMO − 17 and its antibonding counterpart LUMO (Figure 7). HOMO − 17 possesses 12.6% Pt $5d_{z^2}$ character, while the Tl 6s contribution amounts to 4.13%. On the other hand the Pt $5d_{z^2}$ and Tl 6s contributions to the LUMO are 11.1% and 41.3%, respectively. Thus, the Pt−Tl bond formation in $(CN)_4Pt−Tl(dmso)_5^+$ can be simply interpreted as the result of a $Pt(5d^2) \rightarrow Tl(6s)$ donation. The atomic Mulliken charges calculated for Pt and Tl in $Pt(CN)_4^{2-}$ (Pt, 0.09), $Tl(dmso)_5^{3+}$ (Tl, 1.26), and $(CN)_4Pt−Tl(dmso)_5^+$ (Pt, 0.28; Tl, 0.95) provide additional support that the formation of the Pt−Tl bond can be attributed to a transfer of charge from platinum(II) to thallium(III). This bonding scheme is compatible with the very large $^1J_{Pt−Tl}$ coupling constant observed for this system (93 kHz). LUMO + 1 possesses an important Tl 6p contribution (14.6%), while LUMO + 2 contains a very important $5d_{x^2-y^2}$ contribution (42.3%).

The $(NC)_4Pt−Tl(dmso)_5^+$ system constitutes the first example of a Pt−Tl bonded cyanide complex in which the sixth coordination position around Pt (in *trans* with respect to the Tl atom) is not occupied. In fact, the presence of a CN^- ligand in that position was thought to be crucial for the stabilization of the Pt bond. Thus, we also performed an MO analysis on the known $(CN)_5Pt−Tl(dmso)_4$ complex.[20] The Pt−Tl distance calculated for $(CN)_5Pt−Tl(dmso)_4$ (2.655 Å) is 0.080 Å shorter than that calculated for $(NC)_4Pt−Tl(dmso)_5^+$ (2.735 Å). These results clearly confirm that the presence of a fifth cyanide ligand in *trans* position with respect to the Tl atom stabilizes the Pt−Tl bond.

A molecular orbital analysis performed on the $(CN)_5Pt−Tl(dmso)_4$ system shows that the Pt−Tl bond formation in this compound can be also interpreted as the result of a $Pt(5d^2) \rightarrow Tl(6s)$ donation. The main bonding contribution to the formation of the Pt−Tl bond is provided by the HOMO (6.2% Pt $5d_{z^2}$ and 8.3% Tl 6s), the antibonding counterpart being the LUMO (24.5% Pt $5d_{z^2}$ and 28.1% Tl 6s, see Figure S4, Supporting Information). The role of the fifth cyanide ligand in the formation of the Pt−Tl bond may be rationalized by considering the energy of the respective HOFOs in $Pt(CN)_4^{2-}$ and $Pt(CN)_5^{3-}$. The coordination of a CN^- ligand to $Pt(CN)_4^{2-}$ raises the

Table 3. Excited States of $(NC)_4Pt−Tl(dmso)_5^+$ Calculated by TDDFT in Dimethylsulfoxide Solution (PCM Model)[a]

state	composition (excitation amplitudes)[b]	E, nm (eV)	f	assignment
2	HOMO−1 → LUMO (0.44)	376.5 (3.29)	0.067	LMCT
	HOMO−2 → LUMO (0.48)			
3	HOMO−1 → LUMO (0.51)	373.6 (3.32)	0.029	LMCT
	HOMO−2 → LUMO (0.44)			
4	HOMO−3 → LUMO (0.63)	360.2 (3.44)	0.128	LMCT
	HOMO−6 → LUMO (0.21)			
5	HOMO−4 → LUMO (0.31)	346.8 (3.58)	0.031	LMCT + MMCT
	HOMO−5 → LUMO (0.58)			
6	HOMO−3 → LUMO (0.21)	336.7 (3.68)	0.021	LMCT + MMCT
	HOMO−4 → LUMO (0.26)			
	HOMO−6 → LUMO (0.58)			
8	HOMO−4 → LUMO (0.44)	326.4 (3.80)	0.045	LMCT + MMCT
	HOMO−5 → LUMO (0.32)			
	HOMO−6 → LUMO (0.21)			
	HOMO−8 → LUMO (0.32)			
9	HOMO−4 → LUMO (0.25)	314.4 (3.94)	0.068	LMCT + MMCT
	HOMO−8 → LUMO (0.59)			
10	HOMO−9 → LUMO (0.64)	304.3 (4.08)	0.046	LMCT
13	HOMO−11 → LUMO (0.44)	290.8 (4.26)	0.029	LMCT
	HOMO−12 → LUMO (0.51)			
14	HOMO−11 → LUMO (0.28)	288.9 (4.30)	0.072	LMCT
	HOMO−12 → LUMO (0.22)			
	HOMO−13 → LUMO (0.56)			
15	HOMO−14 → LUMO (0.67)	287.7 (4.31)	0.021	LMCT

[a] Only those excited states contributing with $f > 0.02$ are given. [b] Only those excitation amplitudes greater than 0.2 are given.

energy of the HOFO with respect to HOFO − 1 and HOFO − 2 by 2.71 eV. As a consequence, the $Pt(CN)_5^{3-}$ possesses a strong Lewis donor character, resulting in a stronger Pt−Tl bond. This is in line with the larger (Mayer) bond order obtained for Pt−Tl in $(CN)_5Pt−Tl(dmso)_4$ (1.12) in comparison to $(NC)_4Pt−Tl(dmso)_5^+$ (1.03).

TDDFT Calculations. To investigate the absorption spectrum of the $(NC)_4Pt−Tl(dmso)_5^+$ complex in dmso solution we have carried out time-dependent density functional theory (TDDFT) calculations. Indeed, TDDFT has emerged as an accurate method for the calculation of excited state properties of molecules. Because of its low computational cost, TDDFT is applicable to relatively large systems for which traditional wavefunction-based methods are not feasible. Thus, TDDFT appears to be an excellent approach for calculating the electronic spectra of transition metal complexes,[50] including platinum(II) complexes.[51,52] The output of the TDDFT calculations contains information for the excited-state energies and oscillator strengths (f) and a list of the transitions that give rise to each excited state, the orbitals involved, and the orbital contribution coefficients of the transitions. The results are summarized in Table 3. To substantiate the discussion, the molecular orbital
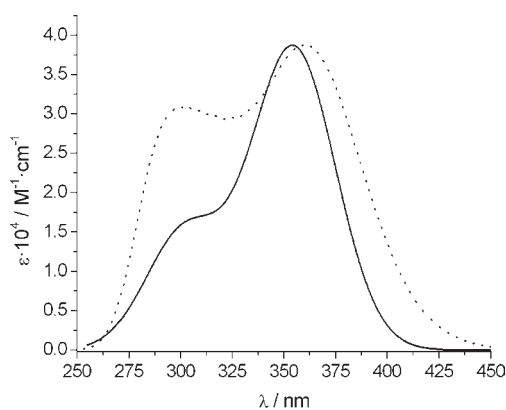
Figure 8. Comparison of the experimental (—) and calculated (TDDFT, · · ·) molar absorption coefficients (ε) of the $(CN)_4Pt-Tl(dmso)_5{}^+$ (A) species. The experimental spectrum was obtained from that shown in Figure 3 $[c_{Pt(CN)_4{}^{2-}} = c_{Tl(dmso)_6{}^{3+}} = 20$ mM] by subtracting the contributions of the unbound species.
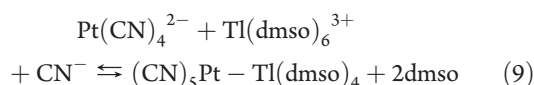
compositions relevant to the interpretation of the absorption spectra are given in Table 2.

The TDDFT calculated spectrum of $(NC)_4Pt-Tl(dmso)_5{}^+$ is compared to the experimental UV–vis spectrum in Figure 8. The agreement between the experimental and calculated spectra is very good. The calculated spectrum presents two maxima at 302 and 361 nm that compare well to those observed in the experimental spectrum (310 and 355 nm). The main discrepancy between the experimental and calculated spectrum is that the calculated one overestimates the intensity of the component at higher energy with respect to the maximum at 361 nm. Table 3 shows the different electronic transitions that provide a relevant contribution to the overall calculated spectrum. It can be seen that the calculated spectrum possesses an important contribution from at least 10 electronic transitions.

Our TDDFT calculations show that the different excited states relevant to the interpretation of the absorption spectrum of the Pt–Tl complex are best described as multi configurations, in which several electron excitations contribute to a given electronic transition. The MO compositions given in Table 2 show that the LUMO is mainly centered on Tl (42.9%), and contains an important Pt contribution (16.7%). HOMO − 1 to HOMO − 3 are mainly centered on the dmso ligands, while HOMO − 8 to HOMO − 16 contain important contributions from dmso and CN^- ligands. A third group of orbitals (HOMO − 4 to HOMO − 7) contain an important contribution from both dmso and CN^- ligands, as well as from Pt (22–30%). Thus, those electronic transitions dominated by excitations from HOMO − 4, −5, −6, and −7 to LUMO can be considered to possess both LMCT and MMCT characters, as the electronic excitation shifts electron charge density from the ligands and Pt to Tl. The remaining electron transitions that do not have relevant contribution from excitations involving HOMO − 4, −5, −6 should be considered as LMCT transitions. The data reported in Table 3 indicate that the low energy band observed in the absorption spectrum contains both LMCT and MMCT character, while the maximum observed at higher energy should be rather considered as an LMCT band.

Absent Reactivity of $(CN)_4Pt-Tl(dmso)_5{}^+$ toward Cyanide in Dimethylsulfoxide. Preparation method for the related compound, $(CN)_5Pt-Tl(dmso)_4$, in dmso solution has previously

been published by Ma et al. according to the following equation:[20]

$$Pt(CN)_4{}^{2-} + Tl(dmso)_6{}^{3+}$$
$$+ CN^- \leftrightarrows (CN)_5Pt-Tl(dmso)_4 + 2dmso \qquad (9)$$

As a matter of fact, when reinvestigating the system we got no evidence for the formation of $(CN)_5Pt-Tl(dmso)_4$ by mixing the three reactants.[53] Moreover, gradually adding larger excesses of CN^- to a solution of $[(CN)_4Pt-Tl(dmso)_5]^+$ in dmso resulted in a decrease of the ^{205}Tl NMR signal intensity of the yellow complex, but no signal of $(CN)_5Pt-Tl(dmso)_4$ ($\delta = 887$ ppm) could be found. In fact, only the signal due to $Tl(CN)_2{}^+$ ($\delta = 2460$ ppm) was observed, which indicates that the Pt–Tl bond is demolished under these conditions.

Keeping in mind that both $(CN)_4Pt-Tl(dmso)_5{}^+$ and $(CN)_5Pt-Tl(dmso)_4$ are well established species, one can expect the following reaction to take place in dmso solution:

$$(CN)_4Pt-Tl(dmso)_5{}^+ + CN^- \leftrightarrows (CN)_5Pt$$
$$-Tl(dmso)_4 + dmso \qquad (10)$$
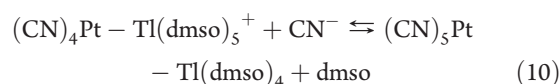
The shorter Pt–Tl bond distance for $(CN)_5Pt-Tl(dmso)_4$ (2.655 Å, calculated by DFT, see Table S1, Supporting Information, or experimental value, 2.6131(4) Å[20]) when compared to $(NC)_4Pt-Tl(dmso)_5{}^+$ (2.735 Å, calculated by DFT) may envisage a thermodynamically favored reaction, i.e., an equilibrium shifted to the right in eq 10. To obtain information about the relative stability of these two Pt–Tl bound species we have determined the free energy for reaction 10 in dmso solution with the aid of DFT. Our calculations provide a free energy calculation in solution $\Delta G° = -95.4$ kJ/mol for reaction 10, which suggests that once the $[(CN)_4Pt-Tl(dmso)_5]^+$ species is formed, the coordination of the fifth cyanide is energetically favored, and the reaction could be therefore inhibited by a high kinetic barrier.

Previous kinetic studies showed that the rate determining step in the formation of the $[(CN)_5Pt-Tl(CN)_n(H_2O)_x]^{n-}$ complexes in aqueous solution is the coordination of the "fifth cyanide" to a $(CN)_4Pt\cdots Tl$ intermediate.[21] However, in aqueous solution (the deprotonated) CN^- ligand has quite high reactivity (at a "stopped flow" time scale), while a similar reaction does not seem to take place at all in dmso. Further work is needed to understand the structural reasoning of this phenomenon.

■ CONCLUSIONS

At first glance, the $(CN)_4Pt-Tl(dmso)_5{}^+$ complex formed in dmso could be considered as a closely related derivative of the growing family of Pt–Tl bonded cyano complexes with general formula $(NC)_5Pt-Tl(CN)_n(H_2O)_x{}^{n-}$ ($n = 0-3$, $x = 5$, 4, 2, 0) prepared earlier by us in aqueous solution.[13–17] However, the detailed study reported herein points to significant differences between these Pt–Tl bond species concerning both structure and bonding. Indeed, the absence of the axial cyanide ligand in the new complex results in a rather unusual square-pyramidal coordination around Pt. Furthermore, several spectral parameters of the $(CN)_4Pt-Tl(dmso)_5{}^+$ complex are remarkably different from the expected ones: (1) The observed $^1J_{Pt-Tl}$ coupling constant (93 kHz) is the largest spin–spin coupling constant ever reported for nonbuttressed Pt–Tl species. (2) The ^{205}Tl NMR shift, $\delta = 75$ ppm, suggests a quite low oxidation state for the Tl-atom. (3) Both the ^{13}C and ^{205}Tl NMR signals are very broad (most likely because of *intra*molecular rearrangement

processes involving the dmso ligands within the complex species with C_1 symmetry). The metal–metal bond formation in $(CN)_4Pt–Tl(dmso)_5^+$ can be simply interpreted as the result of a $Pt(5d_{z^2})^2 \rightarrow Tl(6s)^0$ donation. This bonding scheme may explain the lower thermodynamic stability of this adduct compared to the related complexes containing the $(CN)_5Pt–Tl$ entity, where the linear C–Pt–Tl unit constitutes a very stable bonding system. To our surprise, the $(CN)_4Pt–Tl(dmso)_5^+$ complex does not react with cyanide to give the known $(CN)_5Pt–Tl(dmso)_4$ complex, most likely due to slow kinetics, as the reaction seems to be thermodynamically favored.

The absorption spectrum of $(CN)_4Pt–Tl(dmso)_5^+$ is dominated by two strong absorption bands in the UV region ($\lambda_{max} = 355$ nm, $\varepsilon = 38.7 \times 10^3$ M^{-1} cm^{-1}; $\lambda_{max} = 310$ nm, $\varepsilon = 17.0 \times 10^3$ M^{-1} cm^{-1}) that are assigned to MMCT (Pt $\rightarrow$ Tl) and LMCT (dmso $\rightarrow$ Tl) bands, respectively. The solution of the complex has a bright yellow color (as previously observed for the $(NC)_5Pt–Tl–Pt(CN)_5^{2-}$ trinuclear complex in water)[17,21] as a result of a shoulder present in the low energy side of the band at 355 nm. The complex is light sensitive, and a systematic investigation of its photochemical and photophysical properties is underway.

■ ASSOCIATED CONTENT

ⓢ Supporting Information. Speciation diagrams for the $Pt(CN)_4^{2-}/Tl(dmso)_6^{3+}$ system, ^{13}C NMR titration experiments, orbital interaction diagram for $(NC)_5Pt–Tl(dmso)_4^+$, experimental and calculated bond distances and angles for $(NC)_5Pt–Tl(dmso)_4$, and optimized Cartesian coordinates obtained from DFT calculations. This material is available free of charge via the Internet at http://pubs.acs.org.

■ AUTHOR INFORMATION

Corresponding Author
*E-mail: imretoth@delfin.unideb.hu.

■ ACKNOWLEDGMENT

■ REFERENCES

(1) Nagle, J. K.; Balch, A. L.; Olmstead, M. M. *J. Am. Chem. Soc.* **1988**, *110*, 319–321.

(2) Tóth, I.; Győri, B. In *Encyclopedia of Inorganic Chemistry*, 2nd ed.; King, R. B., Ed.; Wiley: New York, 2005.

(3) Dolg, M.; Pyykkö, P.; Runeberg, N. *Inorg. Chem.* **1996**, *35*, 7450–7451.

(4) Autschbach, J.; Ziegler, T. *J. Am. Chem. Soc.* **2001**, *123*, 5320–5324.

(5) Autschbach, J.; Le Guennic, B. *J. Am. Chem. Soc.* **2003**, *125*, 13585–13593.

(6) Maliarik, M.; Nagle, J. K.; Ilyukhin, A.; Murashova, E.; Mink, J.; Skripkin, M.; Glaser, J.; Kovacs, M.; Horvath, A. *Inorg. Chem.* **2007**, *46*, 4642–4653.

(7) (a) Hao, L.; Vittal, J. J.; Puddephatt, R. J. *Organometallics* **1996**, *15*, 3115–3123. (b) Catalano, V. J.; Malwitz, M. A. *J. Am. Chem. Soc.* **2004**, *126*, 6560–6561. (c) Catalano, V. J.; Bennett, B. L.; Muratidis, S.; Noll, B. C. *J. Am. Chem. Soc.* **2001**, *123*, 173–174. (d) Catalano, V. J.; Bennett, B. L.; Yson, R. L.; Noll, B. C. *J. Am. Chem. Soc.* **2000**,

122, 10056–10062. (e) Hao, L.; Vittal, J. J.; Puddephatt, R. J. *Inorg. Chem.* **1996**, *35*, 269–270. (f) de Silva, N.; Fry, C. G.; Dahl, L. F. *Dalton Trans.* **2006**, 1051–1059. (g) Mednikov, E. G.; Dahl, L. F. *Dalton Trans.* **2003**, 3117–3125.

(8) (a) Chen, W.; Liu, F.; Xu, D.; Matsumoto, K.; Kishi, S.; Kato, M. *Inorg. Chem.* **2006**, *45*, 5552–5560. (b) Oberbeckmann-Winter, N.; Braunstein, P.; Welter, R. *Organometallics* **2004**, *23*, 6311–6318. (c) Stork, J. R.; Olmstead, M. M.; Balch, A. L. *J. Am. Chem. Soc.* **2005**, *127*, 6512–6513. (d) Balch, A. L.; Rowley, S. P. *J. Am. Chem. Soc.* **1990**, *112*, 6139–6140. (e) Balch, A. L.; Fung, E. Y.; Nagle, J. K.; Olmstead, M. M.; Rowley, S. P. *Inorg. Chem.* **1993**, *32*, 3295–3299.

(9) (a) Fornies, J.; Garcia, A.; Lalinde, E.; Moreno, M. T. *Inorg. Chem.* **2008**, *47*, 3651–3660. (b) Fornies, J.; Fuertes, S.; Martin, A.; Sicilia, V.; Gil, B.; Lalinde, E. *Dalton Trans.* **2009**, 2224–2234. (c) Charmant, J. P. H.; Forniés, J.; Gómez, J.; Lalinde, E.; Merino, R. I.; Moreno, M. T.; Orpen, A. G. *Organometallics* **2003**, *22*, 652–656. (d) Fornies, J.; Fortuño, C.; Ibañez, S.; Martin, A. *Inorg. Chem.* **2008**, *47*, 5978–5987. (e) Fornies, J.; Garcia, A.; Lalinde, E.; Moreno, M. T. *Inorg. Chem.* **2008**, *47*, 3651–3660. (f) Falvello, L. R.; Fornies, J.; Garde, R.; Garcia, A.; Lalinde, E.; Moreno, M. T.; Steiner, A.; Tomas, M.; Uson, I. *Inorg. Chem.* **2006**, *45*, 2543–2552. (g) Uson, R.; Fornies, J.; Tomas, M.; Garde, R.; Merino, R. I. *Inorg. Chem.* **1997**, *36*, 1383–1387. (h) Diez, A.; Fornies, J.; Gomez, J.; Lalinde, E.; Martin, A.; Moreno, M. T.; Sanchez, S. *Dalton Trans.* **2007**, 3653–3660.

(10) Jalilehvand, F.; Eriksson, L.; Glaser, J.; Maliarik, M.; Mink, J.; Sandström, M.; Toth, I.; Toth, J. *Chem.—Eur. J.* **2001**, *7*, 2167–2177.

(11) Uson, R.; Fornies, J.; Tomas, M.; Garde, R. *J. Am. Chem. Soc.* **1995**, *117*, 1837–1838.

(12) Chen, W.; Liu, F.; Matsumoto, K.; Autschbach, J.; Guennic, B. L.; Ziegler, T.; Maliarik, M.; Glaser, J. *Inorg. Chem.* **2006**, *45*, 4526–4536.

(13) Berg, K. E.; Glaser, J.; Read, M. C.; Toth, I. *J. Am. Chem. Soc.* **1995**, *117*, 7550–7551.

(14) Maliarik, M.; Berg., K.; Glaser, J.; Sandström, M.; Toth, I. *Inorg. Chem.* **1998**, *37*, 2910–2919.

(15) Jalilehvand, F.; Maliarik, M.; Sandström, M.; Mink, J.; Persson, I.; Persson, P.; Toth, I.; Glaser, J. *Inorg. Chem.* **2001**, *40*, 3889–3899.

(16) Maliarik, M.; Glaser, J.; Toth, I.; Webba da Silva, M.; Zekany, L. *Eur. J. Inorg. Chem.* **1998**, 565–570.

(17) Nagy, P.; Toth, I.; Fabian, I.; Maliarik, M.; Glaser, J. *Inorg. Chem.* **2003**, *42*, 6907–6914.

(18) Maliarik, M.; Glaser, J.; Toth, I. *Inorg. Chem.* **1998**, *37*, 5452–5459.

(19) Maliarik, M.; Plyusnin, V. F.; Grivin, V. P.; Tóth, I.; Glaser, J. *J. Phys. Chem. A* **2008**, *112*, 5786–5793.

(20) Ma, G.; Kritikos, M.; Glaser, J. *Eur. J. Inorg. Chem.* **2001**, 1311–1319.

(21) Nagy, P.; Toth, I.; Fabian, I.; Maliarik, M.; Glaser, J. *Inorg. Chem.* **2004**, *43*, 5216–5221.

(22) Nagy, P.; Joszai, R.; Fabian, I.; Toth, I.; Glaser, J. *J. Mol. Liq.* **2005**, *118*, 195–207.

(23) Ma, G.; Fischer, A.; Glaser, J. *Eur. J. Inorg. Chem.* **2002**, 1307–1314.

(24) Ma, G.; Kritikos, M.; Maliarik, M.; Glaser, J. *Inorg. Chem.* **2004**, *43*, 4328–4340.

(25) Ma, G.; Maliarik, M.; Sun, L.; Glaser, J. *Inorg. Chim. Acta* **2004**, *357*, 4073–4077.

(26) Maliarik, M. *Compounds with Non-Buttressed Metal–Metal Bond between Platinum and Thallium. Model Systems for Photoinduced Two-Electron-Transfer*, Ph.D. Thesis, KTH, 2001; http://kth.diva-portal.org/smash/get/diva2:8942/FULLTEXT01.

(27) Blixt, J.; Győri, B.; Glaser, J. *J. Am. Chem. Soc.* **1989**, *111*, 7784.

(28) Ma, G.; Molla-Abbassi, A.; Kritikos, M.; Ilyukhin, A.; Kessler, V.; Skripkin, M.; Sandström, M.; Glaser, J.; Näslund, J.; Persson, I. *Inorg. Chem.* **2001**, *40*, 6432–6438.

(29) Wolsey, W. C. *J. Chem. Educ.* **1973**, *50*, A335–A337.

(30) Thompson, A.; Attwood, D.; Gullikson, E.; Howells, M.; Kim, K.-J.; Kirz, J.; Kortright, J.; Lindau, I.; Pianatta, P.; Robinson, A.; Scofield,

J.; Underwood, J.; Vaughan, D.; Williams, G.; Winick, H. *X-ray Data Booklet*; LBNL/PUB-490 Rev. 2; Lawrence Berkeley National Laboratory: Berkeley, CA, 2001.

(31) George, G. N.; Pickering, I. J. *EXAFSPAK—A Suite of Computer Programs for Analysis of X-Ray Absorption Spectra*; SSRL: Stanford, CA, 1993.

(32) Becke, A. D. *J. Chem. Phys.* **1993**, *98*, 5648–5652.

(33) Lee, C.; Yang, W.; Parr, R. G. *Phys. Rev. B* **1988**, *37*, 785–789.

(34) Frisch, M. J.; Trucks, G. W.; Schlegel, H. B.; Scuseria, G. E.; Robb, M. A.; Cheeseman, J. R.; Montgomery, J. A., Jr.; Vreven, T.; Kudin, K. N.; Burant, J. C.; Millam, J. M.; Iyengar, S. S.; Tomasi, J.; Barone, V.; Mennucci, B.; Cossi, M.; Scalmani, G.; Rega, N.; Petersson, G. A.; Nakatsuji, H.; Hada, M.; Ehara, M.; Toyota, K.; Fukuda, R.; Hasegawa, J.; Ishida, M.; Nakajima, T.; Honda, Y.; Kitao, O.; Nakai, H.; Klene, M.; Li, X.; Knox, J. E.; Hratchian, H. P.; Cross, J. B.; Bakken, V.; Adamo, C.; Jaramillo, J.; Gomperts, R.; Stratmann, R. E.; Yazyev, O.; Austin, A. J.; Cammi, R.; Pomelli, C.; Ochterski, J. W.; Ayala, P. Y.; Morokuma, K.; Voth, G. A.; Salvador, P.; Dannenberg, J. J.; Zakrzewski, V. G.; Dapprich, S.; Daniels, A. D.; Strain, M. C.; Farkas, O.; Malick, D. K.; Rabuck, A. D.; Raghavachari, K.; Foresman, J. B.; Ortiz, J. V.; Cui, Q.; Baboul, A. G.; Clifford, S.; Cioslowski, J.; Stefanov, B. B.; Liu, G.; Liashenko, A.; Piskorz, P.; Komaromi, I.; Martin, R. L.; Fox, D. J.; Keith, T.; Al-Laham, M. A.; Peng, C. Y.; Nanayakkara, A.; Challacombe, M.; Gill, P. M. W.; Johnson, B.; Chen, W.; Wong, M. W.; Gonzalez, C.; Pople, J. A. *Gaussian 03, Revision C.01*; Gaussian, Inc.: Wallingford CT, 2004.

(35) Ross, R. B.; Powers, J. M.; Atashroo, T.; Ermler, W. C.; LaJohn, L.; Christiansen, P. A. *J. Chem. Phys.* **1990**, *93*, 6654–6670.

(36) (a) Anzellotti, A. I.; Bayse, C. A.; Farell, N. P. *Inorg. Chem.* **2008**, *47*, 10425–10431. (b) Umakoshi, K.; Kojima, T.; Kim, Y. H; Onishi, M.; Nakao, Y.; Sakaki, S. *Chem.—Eur. J.* **2006**, *12*, 6521.

(37) Boehme, C.; Uddin, J.; Frenking, G. *Coord. Chem. Rev.* **2000**, *197*, 249–276.

(38) (a) Cances, M. T.; Mennucci, B.; Tomasi, J. *J. Chem. Phys.* **1997**, *107*, 3032–3041. (b) Mennucci, B.; Tomasi, J. *J. Chem. Phys.* **1997**, *106*, 5151–5158. (c) Mennucci, B.; Cancès, E.; Tomasi, J. *J. Phys. Chem. B* **1997**, *101*, 10506–10517. (d) Tomasi, J.; Mennucci, B.; Cancès, E. *THEOCHEM* **1999**, *464*, 211–226.

(39) Barone, V.; Cossi, M.; Tomasi, J. *J. Chem. Phys.* **1997**, *107*, 3210–3221.

(40) (a) Stratmann, R. E.; Scuseria, G. E.; Frisch, M. J. *J. Chem. Phys.* **1998**, *109*, 8218–8224. (b) Bauernschmitt, R.; Ahlrichs, R. *Chem. Phys. Lett.* **1996**, *256*, 454–464. (c) Casida, M. E.; Jamorski, C.; Casida, K. C.; Salahub, D. R. *J. Chem. Phys.* **1998**, *108*, 4439–4449.

(41) Gorelsky, S. I.; Lever, A. B. P. *J. Organomet. Chem.* **2001**, *635*, 187–196.

(42) This intensity ratio can be observed if the carrier frequency (O1) is taken just at the same distance of the central peak and one of the satellite peaks, i.e., 0 ppm, see insert of Figure 2. (The homogeneous excitation profile cannot be managed due to the huge spectral window needed to record the "quasitriplet", but the above-mentioned position of the carrier frequency ensures equal excitation of the two signals shown in the insert.)

(43) Glaser, J. In *Advances in Inorganic Chemistry*; Sykes, A. J., Ed.; Academic Press: San Diego, CA, 1995, 43, 1−69.

(44) It is also worth mentioning that the Raman vibration band at about 160 cm^{-1} characteristic of the Pt−Tl bond in aqueous solution cannot be observed in dmso. The absence of the Raman band might be a consequence of the lowered symmetry of the Pt−Tl bonded complex in dmso compared to the related species in an aqueous system.

(45) Persson, I.; Jalilehvand, F.; Sandström, M. *Inorg. Chem.* **2002**, *41*, 192–197.

(46) Jalilehvand, F.; Maliarik, M.; Sandström, M.; Mink, J.; Persson, I.; Toth, I.; Glaser, J. *Inorg. Chem.* **2001**, *40*, 3889–3899.

(47) Gutmann, V. *The Donor−Acceptor Approach to Molecular Interactions*; Plenum Press: New York, 1978.

(48) Gielmann, G.; Yershin, H. *Struct. Bonding (Berlin)* **1985**, *62*, 87–153.

(49) Ziegler, T.; Nagle, J. K.; Snijders, J. G.; Baerends, E. J. *J. Am. Chem. Soc.* **1989**, *111*, 5631–5635.

(50) (a) Gorelsky, S. I.; Lever, A. B. P. *J. Organomet. Chem.* **2001**, *635*, 187–196. (b) Sieger, M.; Wanner, M.; Kaim, W.; Stufkens, D. J.; Snoeck, T. L.; Zalis, S. *Inorg. Chem.* **2003**, *42*, 3340–3346. (c) Gross, E. K. U.; Dobson, J. F.; Petersilka, M. *Top. Curr. Chem.* **1996**, *181*, 81–172.

(51) (a) Liu, X.-J.; Feng, J.-K.; Meng, J.; Pan, Q.-J.; Reb, A.-M.; Zhou, X.; Zhang, H.-X. *Eur. J. Inorg. Chem.* **2005**, 1856–1866. (b) Zhou, X.; Zhang, H.-X.; Pan, Q.-J.; Xia, B.-H.; Tang, A.-C. *J. Phys. Chem. A* **2005**, *109*, 8809–8818. (c) Stoyanov, S. R.; Villegas, J. M.; Rillema, D. P. *J. Phys. Chem. B* **2004**, *108*, 12175–12180.

(52) Kadjane, P.; Platas-Iglesias, C.; Ziessel, R.; Charbonniere, L. J. *Dalton Trans.* **2009**, 5688–5700.

(53) Three different experiments have been done: (1) direct mixing of $K_2Pt(CN)_4$, $Tl(dmso)_6^{3+}$, and CN^- in 1:1:1 molar ratio; (ii) preparing 1:1 mixture of $Tl(dmso)_6^{3+}$ and CN^- in dmso followed by adding 1 equiv of $K_2Pt(CN)_4$ in dmso; (iii) preparing 1:1 mixture of $K_2Pt(CN)_4$ and CN^- in dmso followed by adding 1 equiv of Tl-$(dmso)_6^{3+}$ in dmso. In all cases the ^{205}Tl NMR spectra had been recorded at least one day after mixing.

6173

dx.doi.org/10.1021/ic200417q |*Inorg. Chem.* 2011, 50, 6163–6173